AD-A134 749 CRACK PROPAGATION IN POLYSTYRENE UNDER FIXED ELONGATION 1/1
(U) CASE WESTERN RESERVE UNIV CLEVELAND OH DEPT OF
MACROMOLECULAR SCIENCE K SEHANOBISH ET AL. 28 OCT 83
UNCLASSIFIED CWRU/DMS/TR-14 N000M4-75-C-0795 F/G 11/9 NL

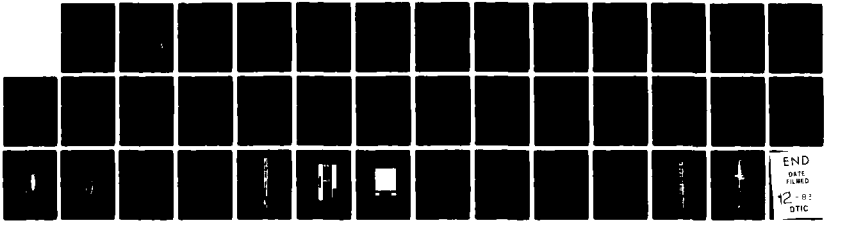

END
DATE FILMED
12-83
DTIC

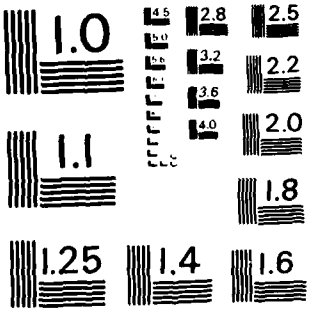

OFFICE OF NAVAL RESEARCH

CONTRACT NO. N00014-75C-0795

PROJECT NO. NR 356-554

TECHNICAL REPORT NO. 14

"CRACK PROPAGATION IN POLYSTYRENE UNDER FIXED ELONGATION"

BY

K. SEHANOBISH, E. BAER, A. CHUDNOVSKY AND A. MOET
DEPARTMENT OF MACROMOLECULAR SCIENCE
CASE WESTERN RESERVE UNIVERSITY
CLEVELAND, OHIO 44106

OCTOBER 28, 1983

SECURITY CLASSIFICATION OF THIS PAGE (When Data Entered)

REPORT DOCUMENTATION PAGE		READ INSTRUCTIONS BEFORE COMPLETING FORM
1. REPORT NUMBER Technical Report #14	2. GOVT ACCESSION NO. AD-A134 749	3. RECIPIENT'S CATALOG NUMBER
4. TITLE (and Subtitle) "Crack Propagation in Polystyrene Under Fixed Elongation"		5. TYPE OF REPORT & PERIOD COVERED Technical Report Interim 6. PERFORMING ORG. REPORT NUMBER
7. AUTHOR(s) K. Sehanobish, E. Baer, A. Chudnovsky and A. Moet		8. CONTRACT OR GRANT NUMBER(s) N00014-75-C-0795
9. PERFORMING ORGANIZATION NAME AND ADDRESS Department of Macromolecular Science Case Western Reserve University Cleveland, Ohio 44106		10. PROGRAM ELEMENT, PROJECT, TASK AREA & WORK UNIT NUMBERS
11. CONTROLLING OFFICE NAME AND ADDRESS Office of Naval Research (Code 472) Arlington, Virginia 22217		12. REPORT DATE October 28, 1983 13. NUMBER OF PAGES
14. MONITORING AGENCY NAME & ADDRESS(if different from Controlling Office)		15. SECURITY CLASS. (of this report) Unclassified 15a. DECLASSIFICATION/DOWNGRADING SCHEDULE

16. DISTRIBUTION STATEMENT (of this Report)
Approved for public release; distribution unlimited. Reproduction in whole or in part is permitted for any purpose of the United States Government.

17. DISTRIBUTION STATEMENT (of the abstract entered in Block 20, if different from Report)

18. SUPPLEMENTARY NOTES

19. KEY WORDS (Continue on reverse side if necessary and identify by block number)
stress-relaxation, fracture, crazing, polystyrene, fractograph, J-integral, energy release rate, fracture toughness, crack propagation.

20. ABSTRACT (Continue on reverse side if necessary and identify by block number)
Microscopic observations of precracked polystyrene samples under fixed elongation conditions reveal that crack propagates discontinuously under diminishing stress to a stable configuration. A zone of intensive crazes in the vicinity of the crack tip evolves concurrently with crack growth. Fracture occurs as the translation and expansion of the crazed zone ahead of the crack. The phenomenon has been successfully explained using a crack layer model. Contrary to conventional fracture mechanics ideas, crack propagation is found

DD FORM 1 JAN 73 1473 EDITION OF 1 NOV 65 IS OBSOLETE
S/N 0102-014-6601

SECURITY CLASSIFICATION OF THIS PAGE (When Data Entered)

to be controlled by the difference between the energy dissipated in damage (crazing) growth and the relevant energy release rate. Conditions of stability have been determined in terms of the relationship between these energies.

CRACK PROPAGATION IN POLYSTYRENE UNDER FIXED ELONGATION

by

K. Sehanobish, E. Baer, A. Chudnovsky and A. Moet

Department of Macromolecular Science

Case Western Reserve University

Cleveland, Ohio 44106

ABSTRACT

Microscopic observations of precracked polystyrene samples under fixed elongation conditions reveal that crack propagates discontinuously under diminishing stress to a stable configuration. A zone of intensive crazes in the vicinity of the crack tip evolves concurrently with crack growth. Fracture occurs as the translation and expansion of the crazed zone ahead of the crack. The phenomenon has been successfully explained using a crack layer model. Contrary to conventional fracture mechanics ideas, crack propagation is found to be controlled by the difference between the energy dissipated in damage (crazing) growth and the relevant energy release rate. Conditions of stability have been determined in terms of the relationship between these energies.

1. Introduction

Studies of the stress relaxation of polymers under relatively large strains are usually directed towards characterizing relaxation modulii and thus the load-bearing capability of the material. Recently, such studies are also used to identify the criteria for the onset of irreversible deformation events [1-5] and to examine environmental effects [6-8]. Although fracture was observed to occur under stress relaxation loading, particularly in the presence of active environments, no attempts to model fracture propagation kinetics in polymers are known to the authors. Perhaps, this is due to the idea that stress generally relaxes to an "equilibrial" level at which the formalism of creep loading may be invoked.

At present, extrapolation of creep rupture curves is a commonly accepted practice for lifetime prediction. Equivalently, curves relating the number of cycles to fail to a given stress (S-N curves) are considered under fatigue loading conditions. This approach obviously rests on the assumption that fracture is a single event. Thus, it ignores the fact that fracture is a complex process involving damage accumulation and interaction on various hierarchical scales prior to ultimate failure. Resulting uncertainties are usually compensated by adopting high safety factors, or relying on expensive prototype testing.

Realizing that crack initiation followed by slow crack propagation are the two major components in the lifetime of an engineering structure, efforts were directed to establish laws of crack propagation. Here, it

is believed that "material" defects may act as crack starters thus determination of crack growth kinetics should suffice to make reasonable lifetime predictions. On the basis of this premise, intensive modelling of fatigue crack propagation has been advanced. Less efforts, however, were directed to develop laws for crack propagation under creep. Even lesser are the attempts to study crack propagation under stress relaxation conditions. Attempts to model crack propagation kinetics under stress relaxation is generally scarce [1] and almost nonexisting for polymers. Formalism of creep crack kinetics, on the other hand, follows the stream of fatigue crack models most of which rests on the original idea of Griffith [9] that fracture propagates as an ideal cut. For example, Gent [10] described creep crack growth in styrene-modified rubber as:

$$\frac{dc}{dt} = 3x10^{-5} \left(\frac{S}{S_o}\right)^3 \qquad (1)$$

where, S and S_o are Griffith's surface energy at any time t and minimum value of surface energy for the crack growth to occur. The front factor and the exponent used in equation (1) were believed to be material constants. Since then several investigators promoted the use of stress intensity factor K to describe creep crack growth in polymers. Relationships of the general form:

$$\frac{dc}{dt} = f(K) \qquad (2)$$

were suggested by many authors [11-14]. Attempts to discover a general law of creep fracture, apart from the actual failure mechanisms, lead to unique

constitutive equations for each of the polymers studied under specific loading conditions. Studying fracture kinetics in precracked structures under fixed displacement is certainly of practical importance. This configuration, in addition, raises interesting questions regarding the nature of crack propagation, if any, under diminishing stress. This paper reports the results of an experiment designed to examine fracture propagation behavior of polystyrene under stress relaxation. Kinetics of the phenomenon is explained in terms of a quantitative account of the concurrently observed mechanisms.

2. Experimental

The material used in this investigation was plane isotropic extruded sheets (0.25 mm thick) of polystyrene obtained from Transilwrap Corporation (Cleveland, Ohio). The draw ratio of the material was approximately 1.8 in the two mutually perpendicular directions. Standard tensile tests showed that the Young's modulus (E) is ≈2.2GPa, the tensile fracture stress is ≈60MPa and the ultimate elongation over 60 mm gauge length is ≈3.5%.

Straight notch of 4 mm depth was introduced into rectangular specimens 20 x 80 mm at a rate of 0.5 mm/min using a razor blade fitted to the crosshead of an Instron machine. The edges were then carefully polished using metallographic techniques to 0.3 μ final finish. Polished samples were annealed in vacuum oven at 90°c for 48 hours and allowed to cool slowly (10°c/hr.) to room temperature.

The tensile behavior of single edge notched (SEN) specimens is

shown in figure 1. The sample was monotonically loaded past the point 'B' (figure 1) at a strain rate of 1.0%/min and then held under fixed elongation. Crack growth and damage evolution were simultaneously observed using a motor driven 35 mm camera attached to a Nikon optical microscope. The microscope-camera assembly was mounted on a movable stage fitted with a micrometer thus providing crack length measurements with precision of a hundredth of a millimeter. Photographs were taken at various stages of relaxation and analyzed.

After 100 hours of stress relaxation the specimen was unloaded, then broken under monotonic loading at a strain rate of 1.0%/min. The fracture surface of the specimen was studied under optical and scanning electron microscopes.

3. Results

Three separate experiments were performed on identical SEN specimens. Although the exact values of the initial conditions (stress and strain) differed slightly from specimen to specimen, the crack propagation mechanism and the stress-relaxation behavior of all three specimens were basically the same. Quantitative analysis provided in this report has been extracted from one experiment.

A semilogarithmic composite plot of the crack growth kinetics and stress relaxation behavior is shown in figure 2. The initial dotted and solid lines indicate crack growth and the corresponding stress rise during the monotonic loading of the specimen. During this period of monotonic

loading the remote stress (at the grips) rises to 26.3 MPa and the crack grows about 0.31 mm. The specimen is then held under fixed grips at this stress level. For the next two hours the test specimen undergoes stress-relaxation accompanied by crack growth. Significant discontinuities in the rate of relaxation and crack growth are observed during this period. The rate of relaxation decreases and then increases while the crack growth rate continues to decrease. At the end of the first two hours the crack growth is abruptly arrested (BC in figure 2) for the next three hours while the stress-relaxation continues to occur (bc). The crack resumes its growth afterwards to be arrested again at point 'D' after which no more crack propagation is observed for the next 80 hours until the experiment is terminated. Although crack ceases to propagate, appreciable reduction in the remote stress is noticed till point 'd' (figure 2) beyond which no significant relaxation could be measured. Finer details of this discontinuous crack growth was clearly revealed from the fractographic analysis as it will be demonstrated later. Figure 3 illustrates how the crack growth rate decays until the final crack arrest occurs at 'D'. The step BC marks the intermediate crack arrest.

An optical micrograph exhibiting a typical side view of the crack and the associated crazed zone is shown in figure 4. Contrary to the dominantly accepted image of an ideal cut, the crack propagates preceded by a layer of intense crazed zone displaying "candle flame" pattern. Concurrent with the stress-relaxation, the crazed zone translates and expands. A halo of diffuse surface crazes (region 'H' in figure 4) slowly begins to

appear surrounding the leading front of the intense crazed zone. The "halo" crazes spread over the entire specimen with time. Crack propagation, however, occurs through the most intense part of the candle flame crazed zone.

A more lucid view of the interaction between craze growth and crack propagation is illustrated in figure 5. The figure exhibits the evolution of the crack and the crazed zone as directly traced from optical micrographs similar to that of figure 4 but magnified 1.5 times. Points A to F (figure 5) indicate the locations of the crack tip at various stages of relaxation. During the initial stages of relaxation, advancement of the crack tip is always accompanied by advancement of the crazed zone tip (points A_1, B_1, C_1) until the crack is arrested at C. This crack arrest corresponds to the first visible crack arrest indicated in figure 2 (BC). Although the crack remains arrested at C for three hours the crazed zone propagates from C_1 to C_2. During this period the material undergoes considerable relaxation as indicated in figure 2. Once more the crack resumes its growth to be arrested again at location F (figure 5). Similar to the first crack arrest at C, the candle flame crazed zone continues its propagation with time from F_1 to F_2. This craze growth also results in considerable stress-relaxation although at a decaying rate.

A more detailed understanding of the crack-crazed zone propagation can be gained by considering the geometric evolution of the crazed zone. As shown in figures 4 and 5, the crazed zone appears to be approximately elliptical in shape and can be characterized by its major and minor axes.

Figure 6 indicates that $\ell_a(t)$ and $w(t)$ normalized with respect to the final values ℓ_a and w, i.e., $\frac{\ell_a(t)}{\ell_a}$ and $\frac{w(t)}{w}$, respectively increase with crack length in a monotonic fashion. The ratio of crazed zone length to width remains nearly constant during the entire history studied. This indicates that the crazed zone expands in a self similar manner irrespective of the discontinuous crack growth.

After 100 hours of stress-relaxation, the specimen was unloaded and then loaded at the same strain rate (1.0%/min) to fracture. The relationship of the remote stress (load divided by the initial cross-sectional area) to the overall elongation is shown in figure 7. It interesting to note that the stress strain behavior now shows an ini "toe region" where the change in stress with respect to strain, $\frac{d\sigma}{d\varepsilon}$, [illegible]ly increases. Through a smooth transition, the toe region is followed by a linear region of constant effective modulus (1.65 GPa) prior to fracture. Note that this effective modulus is considerably lower than the elastic modulus of the notched sample prior to crack-craze propagation (2.1 GPa). This behavior clearly reflects the microstructure of the crazed zone and the associated crack growth.

Optical micrographs of the fracture surface taken from the region of slow crack propagation is shown in figure 8A. It is generally recognized that fracture surface striations are caused by discontinuous crack advance. This discontinuous crack growth pattern is well documented here by the striated morphology of the fracture surface (figure 8A). The first striation indicated by the arrow 'A' on the fractograph corresponds

to crack length measured after 6 minutes (figure 2). The absence of striation prior to 'A' indicates that crack growth was not immediately interrupted upon stopping the movement of the crosshead. Although only two complete crack arrests were observed from kinetic measurements (figure 2), detailed microscopic study of the fracture surface reveals the presence of seven distinct striations. Striations indicated by arrows A,C, D,E, and F are obviously caused by short duration crack arrests. Instead of appearing as clear steps (eg. B-C in figure 2) they appear as discontinuities in crack growth rate (between points A to B in figure 2). No more striations were noticed beyond 1.7 mm from the notch tip. This agrees fairly well with the ultimate crack arrest between points D to E of figure 2.

At a distance of 2.1 mm from the striation G, a curved striation 'H' associated with a sharp morphological change is observed. This curved striation usually corresponds to the transition from slow crack growth to avalanche-like (uncontrolled) crack propagation [13]. This transition involves large scale tearing of drawn material (arrow 'T' in figure 8B). Elliptical fissures grown perpendicular to the fracture surface are observed within the transition region (figure 8c). Critical crack length corresponding to the uncontrolled crack propagation has been identified (arrow 'C' in figure 13B) by correlating the side view with the fracture surface.

4. Discussion

The results described above reveal the nature of fracture propagation under stress relaxation conditions and raise several important questions, most

of which is addressed in this section. The first deals with identifying the forces driving this complex process.

In linear elastic fracture mechanics (LEFM), formulation of criteria for crack growth is based on the energy release rate G, consequently when crack extension occurs G should increase with crack growth rate. The energy release rate G has been calculated from our experimental results as

$$G = \frac{\sigma^2 \pi \ell}{E} f^2\left(\frac{\ell}{B}\right) \qquad (3)$$

Here, G is the remote stress, E is the Young's modulus, ℓ is the crack length and B is the width of the specimen. The geometric function $f(\frac{\ell}{B})$ has been evaluated according to the elastic solution of the boundary value problem [15].

$$f\left(\frac{\ell}{B}\right) = 1.12 - 0.231\left(\frac{\ell}{B}\right) + 10.55\left(\frac{\ell}{B}\right)^2 - 21.72\left(\frac{\ell}{B}\right)^3 + 30.39\left(\frac{\ell}{B}\right)^4 \qquad (4)$$

The average crack growth rate $\dot{\ell}$ as a function of G is shown in figure 9. The energy release rate G may explain the growth kinetics in very small regions. It certainly is unable to explain the entire history of propagation. Clearly, G cannot be taken as the driving force for crack propagation. The demonstrated inadequacy of LEFM to the present case stems from the basic idea that fracture advances as an ideal crack cut. This idea was first introduced by Griffith [9] to model crack propagation in inorganic glass, a truly brittle material. However, it is quite evident from the observed results that the crack does not propagate as an ideal cut.

The crack propagates preceded by a layer of intense craze zone (Figs. 4 & 5).

Damage continues to accumulate in the form of crazes in this zone until a critical level is reached when the entire system i.e. the crack-craze zone becomes unstable and translates to a new configuration. This process is repeated during the fracture process until it reaches a stable configuration (Fig. 5).

Ductile fracture mechanics is promoted in recognition of the damage associated with the crack tip. Recently the line plastic zone model proposed by Dugdale [16] and Barenblatt [17] has gained wide yet controversial applicability to polymers [18-23]. Several authors [24-25] have correlated the band width on the fracture surface to the Dugdale plastic zone size. This implies that the crack advances through a single craze ahead of tip. Accordingly, the band width should increase with G. Figure 10, however, illustrates that the band width measured from the fracture surface (Fig. 10) behave quite oppositely. Hence, ductile fracture mechanics based on the idea of a line plastic zone may not be applicable to our case.

It may be argued that the damage preceding the crack (Fig. 4) can be treated as plastic zone. Consequently, one may calculate the J-integral [27,28] as a possible driving force. A solution of J for our problem is not available in the current literature. Therefore, we make use of an alternate approach to evaluate J-integral. It well recognized that the energy release rate can be expressed as

$$J = - \frac{\partial P}{\partial \ell} \qquad (4)$$

The remote displacement Δ at the grips is evaluated from knowledge of craze zone geometry, craze density and crack opening displacement using Green's function

[29]. The potential energy can then be directly evaluated from

$$P = \tfrac{1}{2} F\Delta \qquad (5)$$

for a fixed grip condition, where F is the Force at the grips. Details of these calculations will appear in a forthcoming publication. The energy release rate "J" so calculated is plotted as a function of the crack growth rate "$\dot{\ell}$" (Fig. 11). Notable, $\dot{\ell}$ vs J relationship is similar to $\dot{\ell}$ vs G (Fig. 9). It is therefore obvious that conventional fracture mechanics approaches cannot account for the observed crack propagation. This paradox can be resolved when one re-examines the mechanism of fracture. Figures 5 and 6 clearly show that fracture propagates as translation and expansion of the crack-craze zone. In addition, it is also observed that motion of the crack-craze system occurs only upon the accumulation of certain level of damage. The energy expended in damage expansion and densification is not incorporated in conventional fracture mechanics.

In a recent development [30-32] this phenomena has been successfully explained considering the crack and the craze zone as a single thermodynamic entity-crack layer (CL). Propagation of the CL may involve combination of elementary movements such as translation, rotation, isotropic expansion and/or shape changes. The configuration of the CL may be assumed to be stable at certain stages during which damage accumulates within the crazed zone defined as the <u>active zone</u>. When instability conditions are satisfied, the active zone jumps into a new configuration. Repetition of this evolutionary process constitutes fracture propagation. Considering the observed geometric evolution of the active zone (Fig. 6) we may conclude that CL propagation

only involves translation and expansion. A closer look at figure 5 confirms this fact because when the crack remains arrested the active zone continues to grow. The entropy production rate associated with the CL propagation can be expressed in the following bilinear form [37-39].

$$T\dot{S} = \dot{D} + \dot{\ell}\, x^{(\ell)} + \dot{e}\, x^{(e)} \tag{6}$$

Here, the rates of CL extension $\dot{\ell}$ and expansion $\dot{e}$ are the thermodynamic fluxes conjugated with thermodynamic forces $x^{(\ell)}$ and $x^{(e)}$, and $\dot{D}$ is the rate of energy dissipated in damage formation and growth. In order to explain the abnormal crack growth kinetics displayed in figure 3, only translational component $x^{(\ell)}$ of the pair of driving forces mentioned above is considered. For CL propagation by translational mode alone equation (6) reduces to

$$T\dot{S} = \dot{D} + \dot{\ell}\, x^{(\ell)} \tag{7}$$

Here the driving force $x^{(\ell)}$ is derived as [32]

$$x^{(\ell)} = \gamma^* R_1 - J \tag{8}$$

where, γ^* is the specific enthalpy of damage and R_1 is the translational resistance moment of the CL which can be evaluated as an average crazing density $\langle\rho\rangle$ times the crack layer width, i.e., $R_1 = \langle\rho\rangle\, w$. An effective enthalpy of damage $\gamma (= {}^*\gamma\, \langle\rho\rangle)$ for the same material was found to be 12×10^3 KJ/m^3 [33]. Thus, $\gamma^* R_1$ was evaluated as a product of γ and the crack layer width (w) obtained from our experiments (Fig. 5). The J values plotted in figure 11 were employed to calculate the driving force $x^{(\ell)}$ in equation (8). Since the thermodynamic fluxes are reciprocally related to their forces, the crack growth rate "$\dot{\ell}$" scales with $1/x^{(\ell)}$. An increase in $x^{(\ell)}$ should therefore result in a decay of crack growth rate. This

prediction is clearly evident from figure 12 where $\dot{\ell}$ has been plotted against the $x^{(\ell)}$ evaluated from our experiment. Hence, the actual driving force governing the crack growth kinetics (Fig. 3) has been identified.

The unusual stress-strain behavior of the specimen after 100 hours of stress-relaxation is another striking observation that needs explanation. An initial "toe region" has been displayed (Fig. 7) and subsequently the percent elongation to fracture increases. The significant difference in stress-strain behavior between the samples with (Fig. 7) and without (Fig. 1) a prior history of stress-relaxation must be a consequence of the extent of crazing. Figures 13A and B show the extent of crazing induced in the initial sample and in stress relaxed sample after monotonic fracture, respectively. The extent of crazing in the latter explains the stress-strain behavior. Related precrazing effects have been recently reported [34,35].

Knowledge of the fracture stress (Fig. 13) and the critical crack length yield critical energy release rates of 11.6 KJ/m^2 for case A and 36.3 KJ/m^2 for B. This lends further support to the CL theory since equations (7 and 8) yield

$$Jc = \gamma^* R_{1c} \tag{9}$$

for critical crack propagation [33]. Accordingly, the critical energy release rate "J_c" should depend on the extent of damage expressed as $R_1 (=\langle\rho\rangle w_c)$. The critical width of the active zone w_c for the relaxed specimen (at arrow C in Fig. 13B) is estimated as three times that of the initial specimen at the notch tip, Fig. 13A. Thus, the three fold increase in fracture toughness is directly related to a similar increase in the extent of crazing.

History dependence of the critical energy release rate has been recently documented [33,36].

5. Conclusions

i) Discontinuous crack propagation occurs under stress relaxation loading even below the monotonic crack initiation stress. The crack is always preceded by a dense crazed zone. Fracture advances as interactive leaps of the crazed zone and the crack.

ii) The fracture processes are successfuly explained using the crack layer theory. The actual driving force (cause) of the observed fracture was defined in terms of the difference between the amount of energy "$\gamma^* R_2$" required for the active zone advance and the amount energy available for the process (the energy release rate "J").

iii) Evidence is presented to show the existence of hydrostatic tension ahead of fast moving cracks.

iv) The presence of the crazed zone ahead of the crack is found to increase the critical energy release rate (fracture toughness) markedly.

References

1. S.S. Sternstein, L. Ougchin, A. Silverman, Applied Pol. Symposia, 7 (1968) 175.

2. E.J. Kramer and R.A. Bubeck, J. Polym. Sci. Polym. Phys., Ed. 16 (1978) 1195.

3. O.S. Bruller, Polymer, 19 (1978) 1195.

4. A.S. Argon and M.M. Salama, Philos. Magazine, 36, 5 (1977) 1217.

5. J.B.C. Wu and N. Brown, J. Rheology, 23.2 (1979) 231.

6. A.S. Moet, I. Palley, E. Baer, J. Appl. Phys., 51 (1980) 10.

7. L.H. Tung, J. Polym. Sci., A, 3 (1965) 1845.

8. E. Gaube, Kunststoffe 49 (1959) 446.

9. A.A. Griffith, Philos. Trans. Soc. (London) 19, (1979) 8.

10. A.N. Gent and H. Hirakawa, J. Polym. Sci., A 2, 6, (1968) 1481.

11. G.P. Marshall, L.E. Culver and J.G. Williams, Plastics Polym. (1975) 1969.

12. W.G. Knauss, Int. J. Fract. Mech., 6 (1970) 7.

13. M. Kilagawa and K. Motomura, J. Polym. Sci. Polym. Phys., 12 (1974) 1979.

14. S.R. Price and D. Hull, J. Mat. Sci., 18 (1983) 2795.

15. H. Tada, P.C. Paris and G.P. Irwin, The Stress Analysis of Cracks Handbook, Del. Research Corporation, Helertown, Pa., 1973.

16. D.S. Dugdale, J. Mech. Phys. Sol., 8 (1960) 100.

17. G.I. Barenblatt, Adv. in Appl. Mech., 7 (1962) 55.

18. H.R. Brown and I.M. Ward, Polymer, 14 (1973) 469.

19. M.J. Doyle and J.G. Wagner in proceedings of ACS symposium on toughness and brittleness of plastics, Sept. 1976, edited by R.D. Deanin and A.D. Crugnola in chemistry series 154(ACS) p.63.

References (Cont'd)

20. W. Doll, G.W. Weidmann, Prog. Colloid. Polym. Sci., 66 (1979) 291.

21. S.J. Israel, E.L. Thomas and W.W. Gerberich, J. Mat. Sci., 14 (1979) 2128.

22. W. Wang and E.J. Kramer, J. Mat. Sci., 17 (1982) 2013.

23. W. Doll, U. Shiedelmann, K. Konczol, J. Mat. Sci., 15 (1980) letters 2389.

24. R.W. Hertzberg, Int. J. Fract., 15, 2 (1979).

25. J.P.E. Link, J.C. Baumens and G. Howes, Int. J. Fract. Mech., 7 (1971) 277.

26. R. Schirrer, R. Lang, J. Manson B. Tomatis, submitted to fourth Cleveland symposium of macromolecules, Case Western Reserve University, June 13-15, 1983.

27. J.R. Rice, J. Appl. Mech., 35 (1968) 379.

28. G.P. Cherepanov, J. Appl. Math. and Mech. translation 31 (1967) 304.

29. A. Duglaposky, Ph.D. thesis, Civil Engg., Case Western Reserve University, 1983.

30. A. Chudnovsky, NASA report, in press.

31. A. Moet, A. Chudnovsky, Polym. Eng. Sci. (1982) 84.

32. A. Chudnovsky and A. Moet, submitted to the sixth international conference on fracture, New Dehli, India 1984.

33. N. Haddoui, A. Chudnovsky and A. Moet, Polym. Mat. Eng. Sci., 49 (1983) 117.

34. A. Moet, I. Palley, E. Baer, J. Appl. Phys., 10 (1980) 51.

35. M.E. Mackay, T.G. Teng and S.M. Schultz, J. Mat. Sci., 14 (1979) 221.

36. M. Bakar, A. Moet, and A. Chudnovsky, Int. conference of fatigue in polymers, The rubber and plastic institute, London, June (1983) paper no. 8.

Acknowledgment

The authors gratefully acknowledge the financial support of the Office of Naval Research (ONR) through grant number N000-14-75-C-0795.

FIGURE CAPTIONS

Figure 1: Stress-elongation diagram of SEN polystyrene samples. Arrows 'A' and 'B' point to craze initiation and crack initiation, respectively.

Figure 2: Composite plot of stress-relaxation behavior and crack growth kinetics in precracked PS. Crack grows discontinuously under decreasing stress.

Figure 3: Crack growth rate "$\dot{\ell}$" versus crack length. Step BC corresponds to intermediate crack arrest.

Figure 4: Optical micrograph displaying the evolution of "through" crazes surrounding the crack tip. Zone 'H' consists of diffused surface crazes.

Figure 5: Composite plot showing crack growth and evolution of the crazed zone. Vertical markers (A through F) indicate crack tip positions.

Figure 6: Plots of the ratio of instantaneous active zone length $[\ell_a(t)]$ to final length $[\ell_a]$ and the ratio of instantaneous active zone width $[w(t)]$ to the final width $[w]$ versus crack length.

Figure 7: Stress-elongation behavior of the relaxed specimen after unloading.

Figure 8A: Optical micrograph of the fracture surface displaying discontinuous crack growth bands A through G during stress-relaxation of 100 hours. Arrow 'H' indicates the location where the curved striation terminates signaling uncontrolled crack propagation during subsequent monotonic loading.

Figure 8B: Scanning electron micrograph of the fracture surface showing large scale tearing (arrow T) of the drawn material associated with striation 'H' in figure 8A. Horizontal arrow indicates the crack propagation.

Figure 8C: Scanning electron micrographs of the fracture surface showing the elliptical fissures grown perpendicular to the fracture surface.

FIGURE CAPTIONS (Cont'd)

Figure 9: Energy release rate G versus crack growth rate $\dot{\ell}$.

Figure 10: Relationship of fracture band widths to the energy release rate (dotted line) compared with the predicted (solid line).

Figure 11: Change in energy release rate 'J' as a function of crack growth rate $\dot{\ell}$.

Figure 12: Crack growth rate $\dot{\ell}$ versus translational driving force $X^{(\ell)}$. (see text)

Figure 13A: Side view of the fractured surface corresponding to the stress-elongation diagram in figure 1.

Figure 13B: Side view of the fractured surface corresponding to the stress-elongation diagram in figure 7.

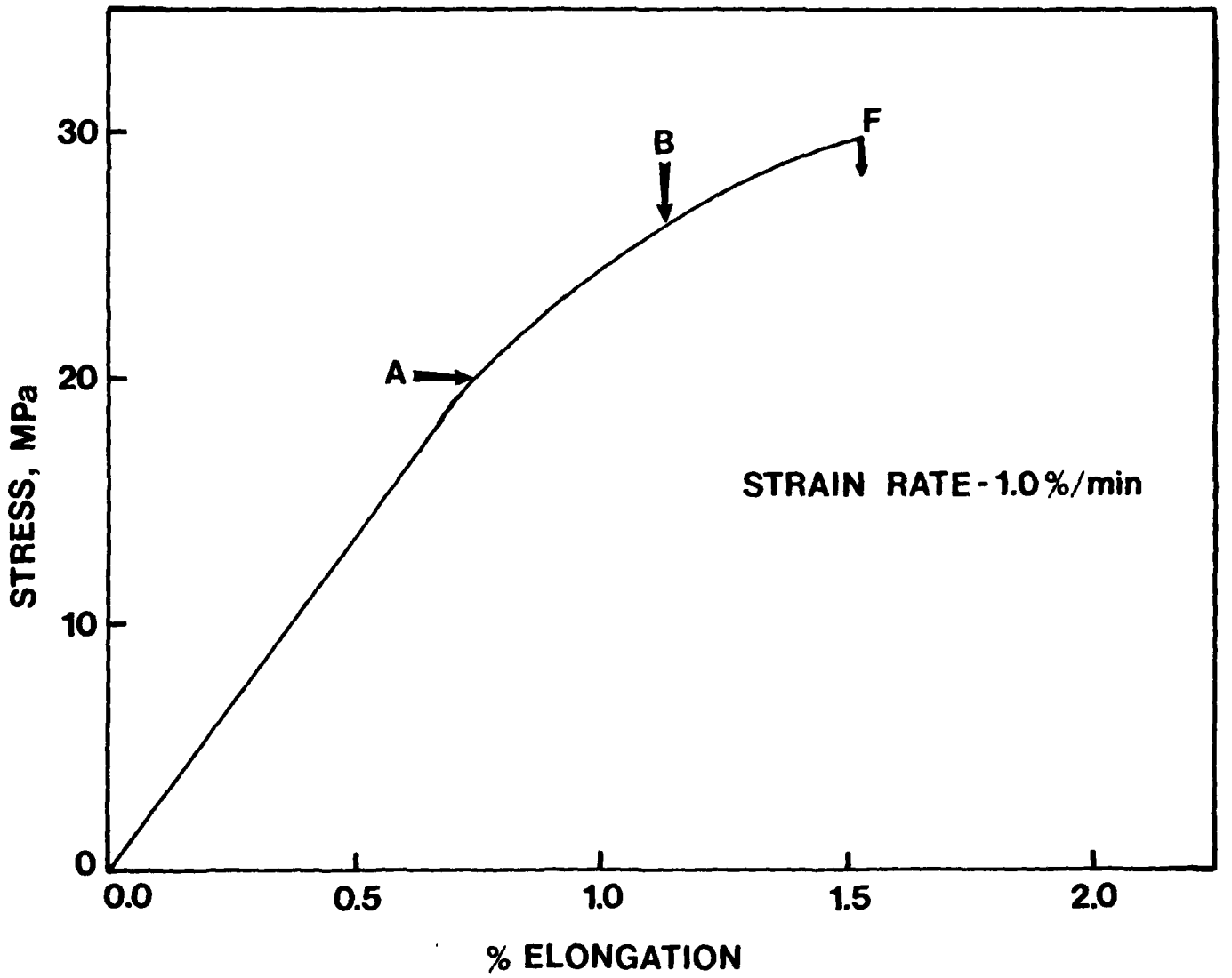
30
20
10
0
STRESS, MPa
A
B
F
STRAIN RATE - 1.0 %/min
0.0
0.5
1.0
1.5
2.0
% ELONGATION

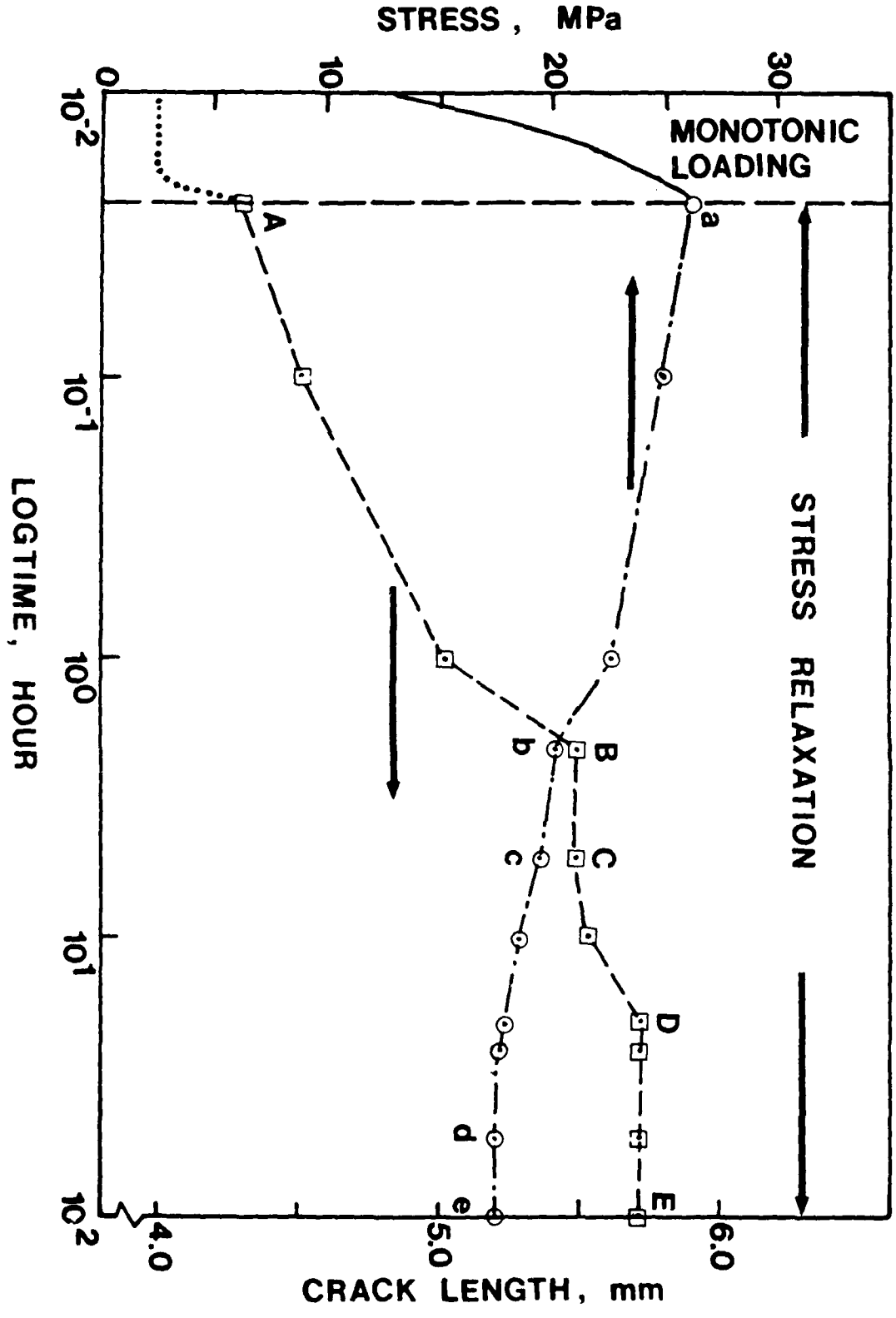
STRESS , MPa
0
10
20
30
MONOTONIC LOADING
A
a
b
B
c
C
D
d
e
E
STRESS RELAXATION
LOGTIME, HOUR
10^{-2}
10^{-1}
10^{0}
10^{1}
10^{2}
4.0
5.0
6.0
CRACK LENGTH, mm

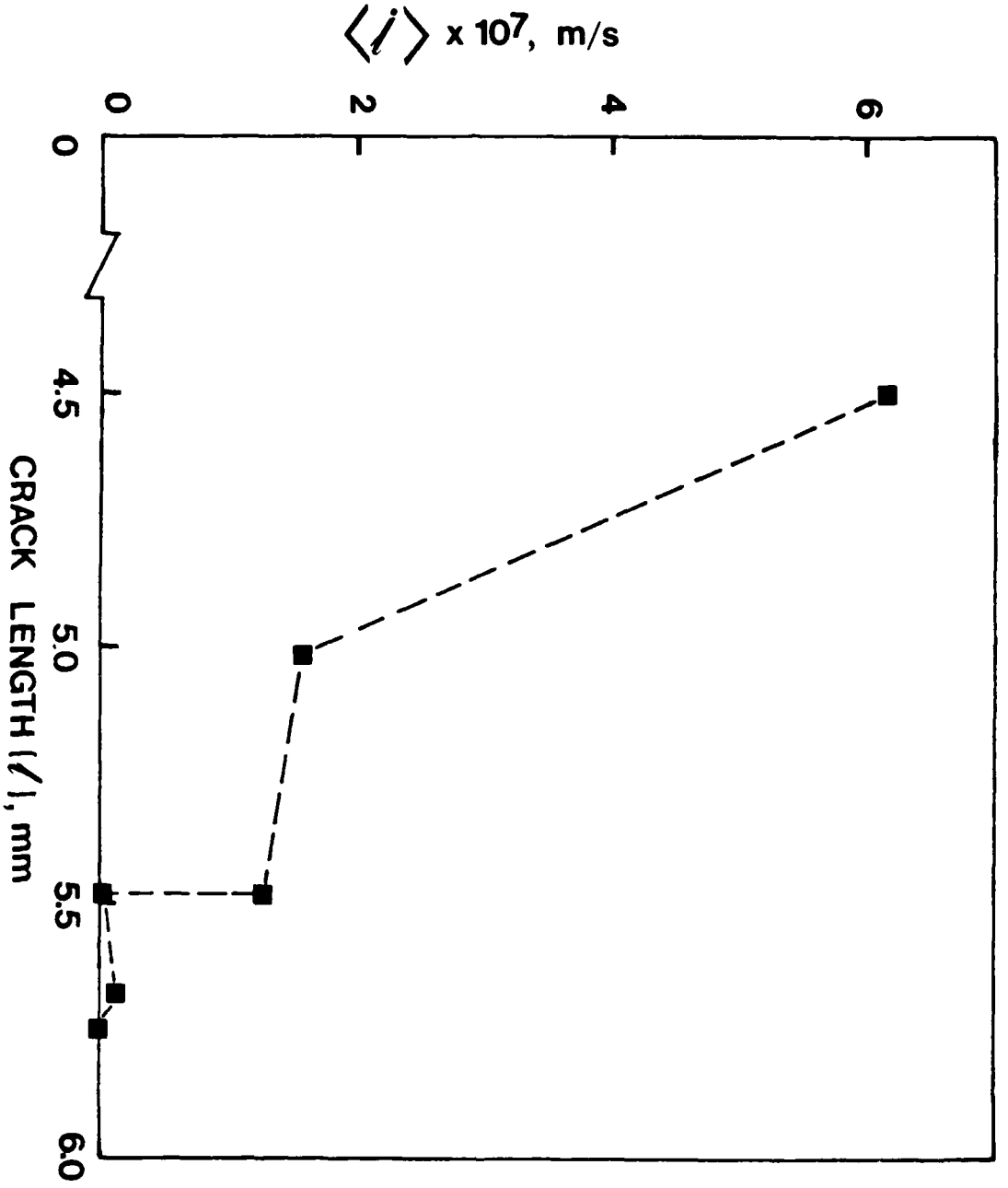
⟨i⟩ x 10⁷, m/s
0
2
4
6
0
4.5
5.0
5.5
6.0
CRACK LENGTH (ℓ), mm

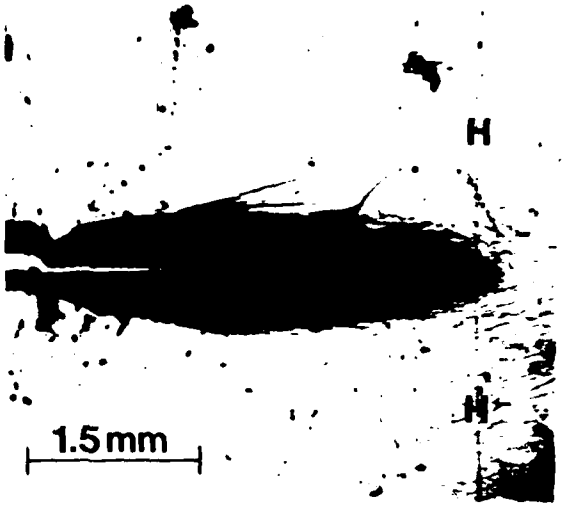
H
H
1.5mm

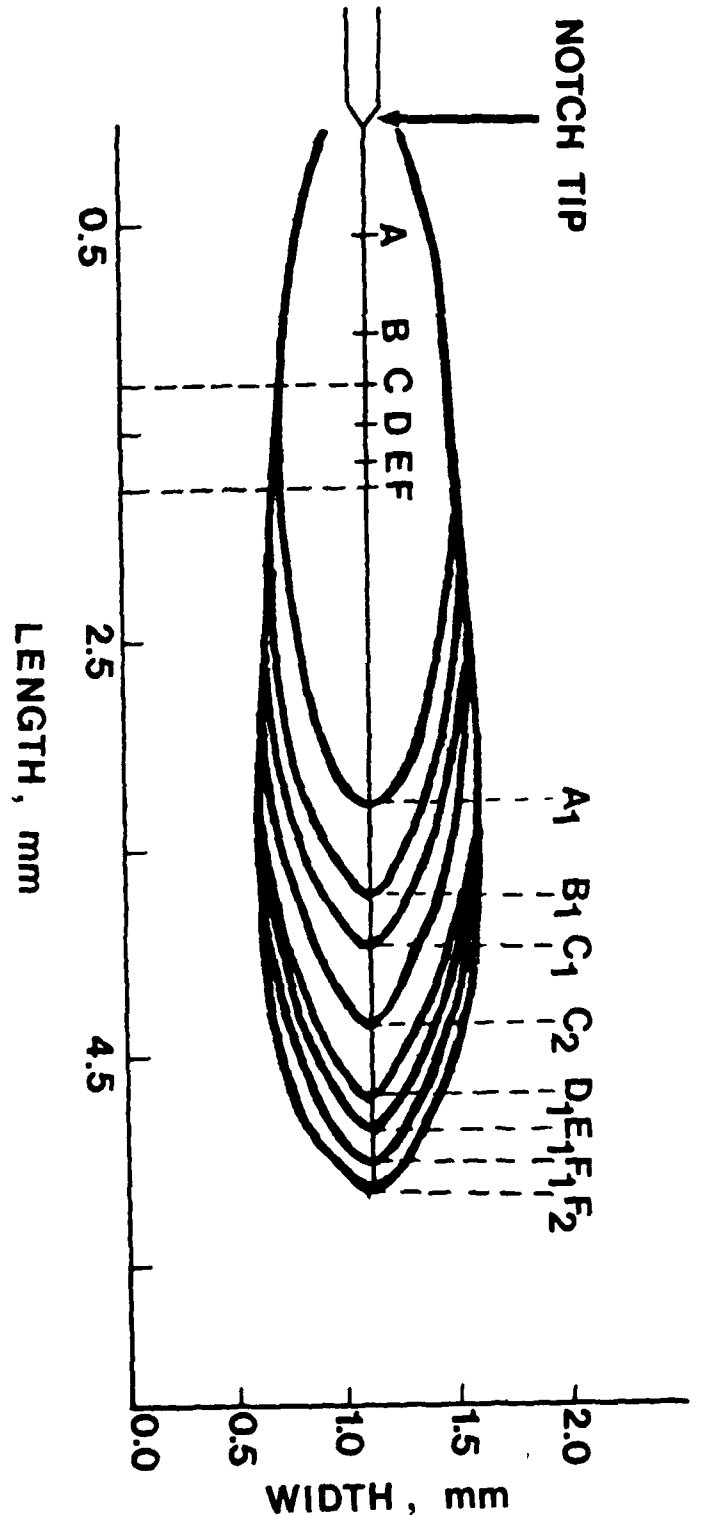
NOTCH TIP
A
B
C
D
E
F
A1
B1
C1
C2
D1
E1
F1
F2
0.5
2.5
4.5
LENGTH, mm
0.0
0.5
1.0
1.5
2.0
WIDTH, mm

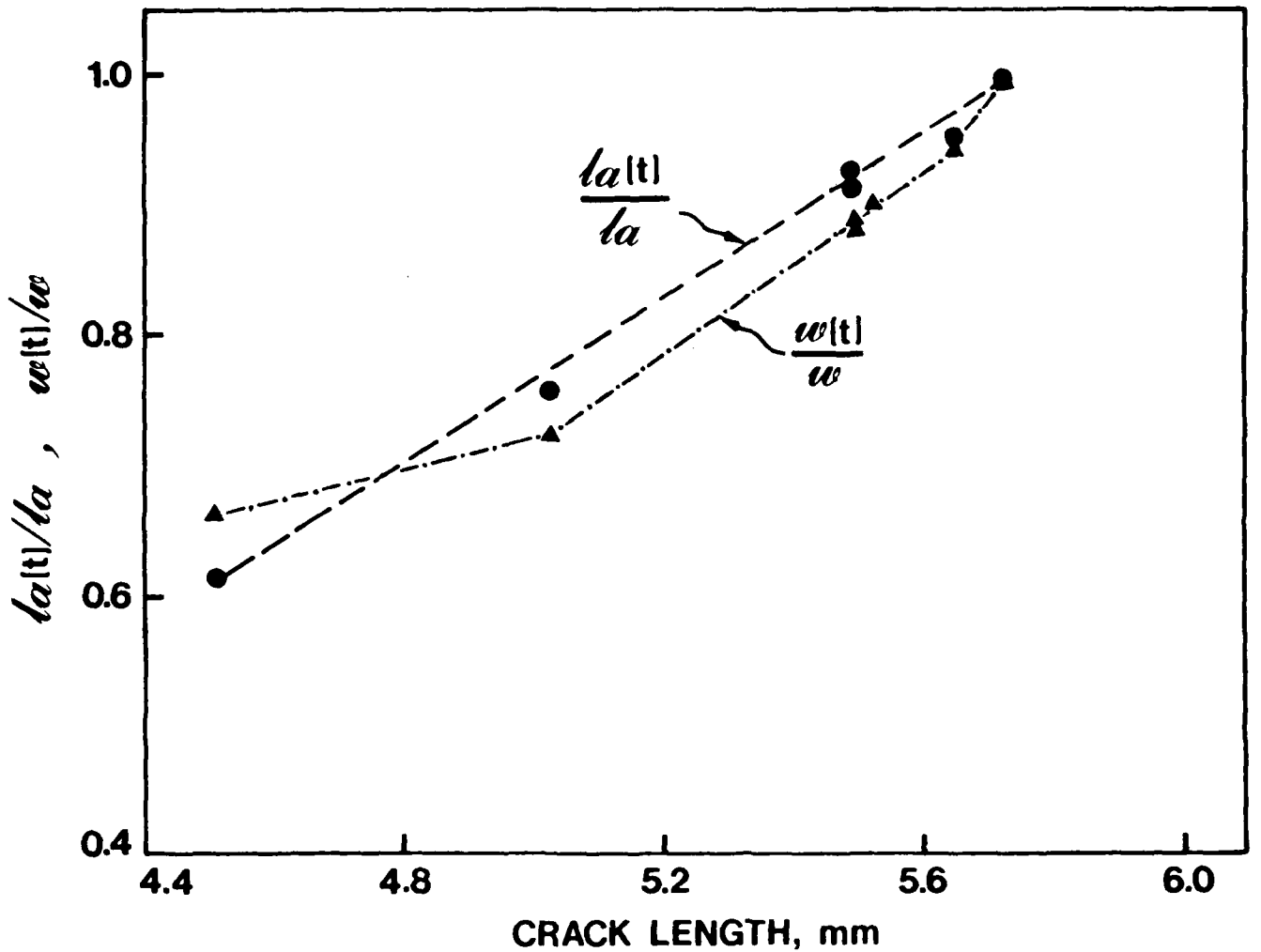
1.0
0.8
0.6
0.4
4.4
4.8
5.2
5.6
6.0
CRACK LENGTH, mm
la[t]/la , w[t]/w
la[t]/la
w[t]/w

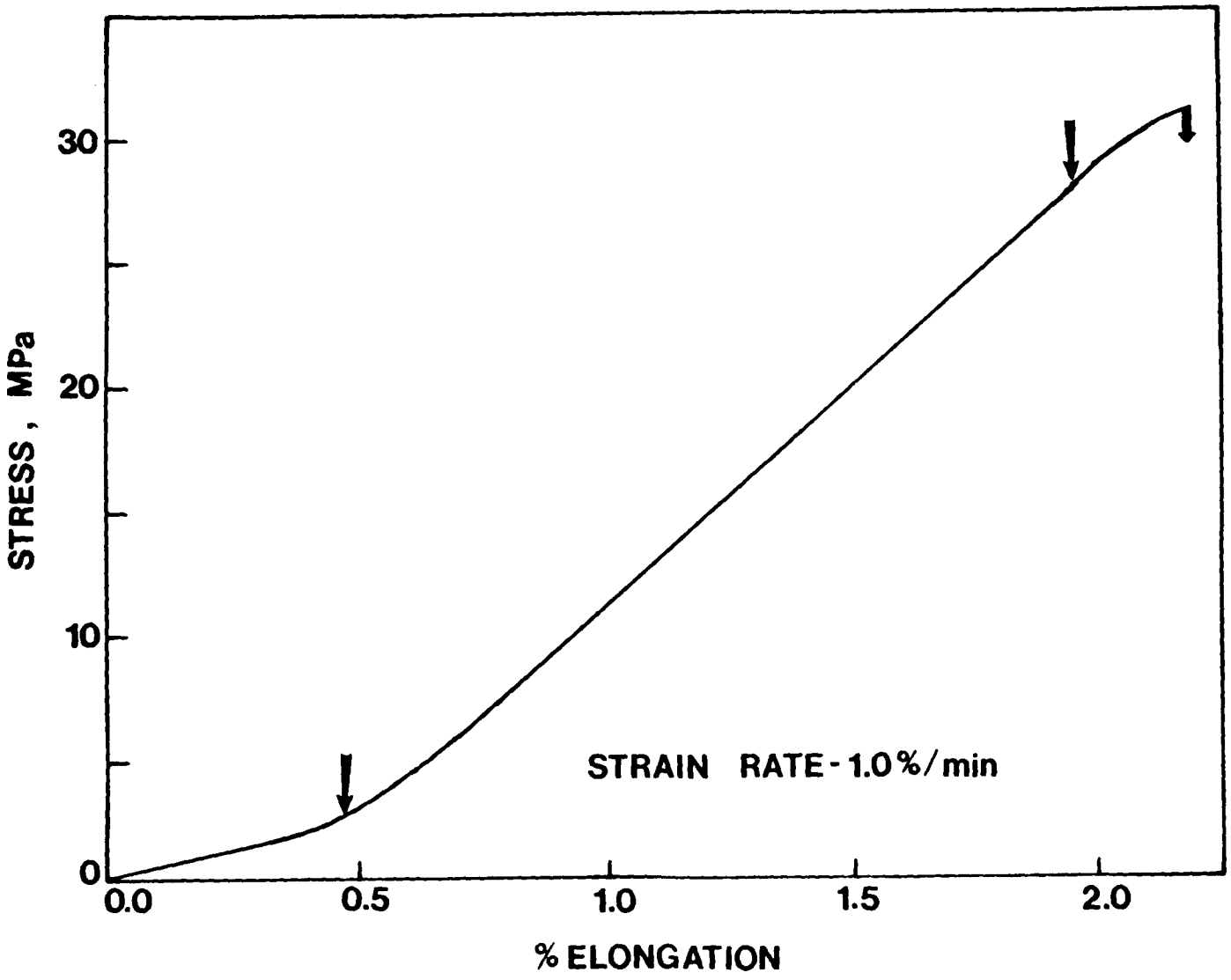
30
20
10
0
STRESS, MPa
STRAIN RATE - 1.0%/min
0.0
0.5
1.0
1.5
2.0
% ELONGATION

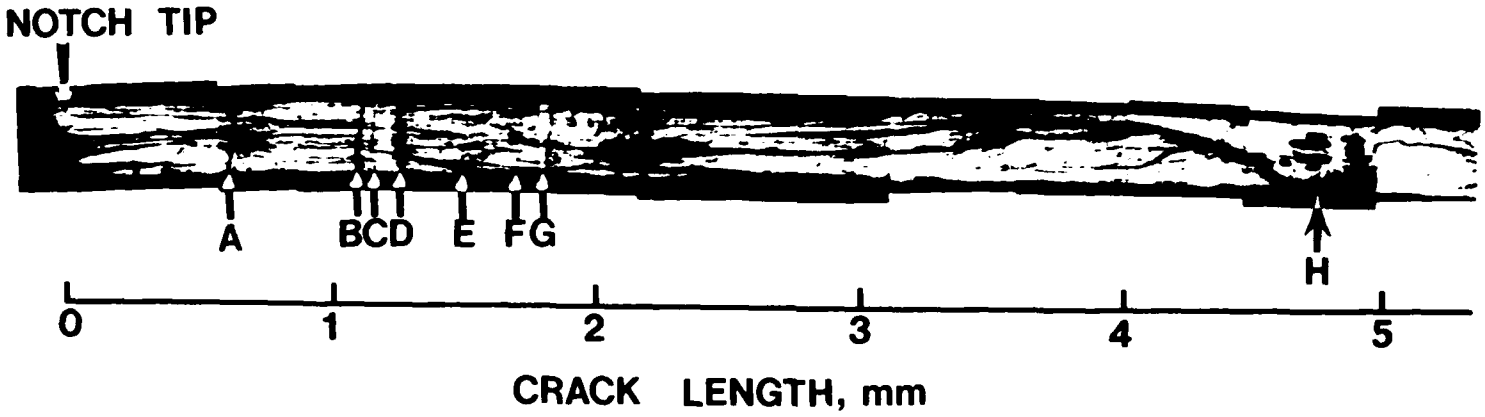
NOTCH TIP
A
BCD
E
FG
H
0
1
2
3
4
5
CRACK LENGTH, mm

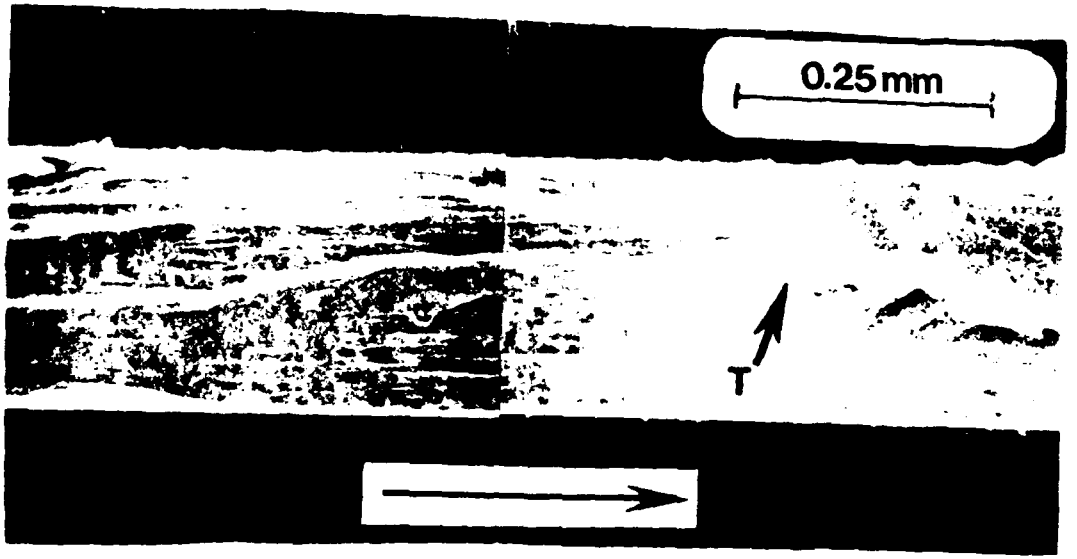
0.25 mm
T

35KV X330 0000 100.0

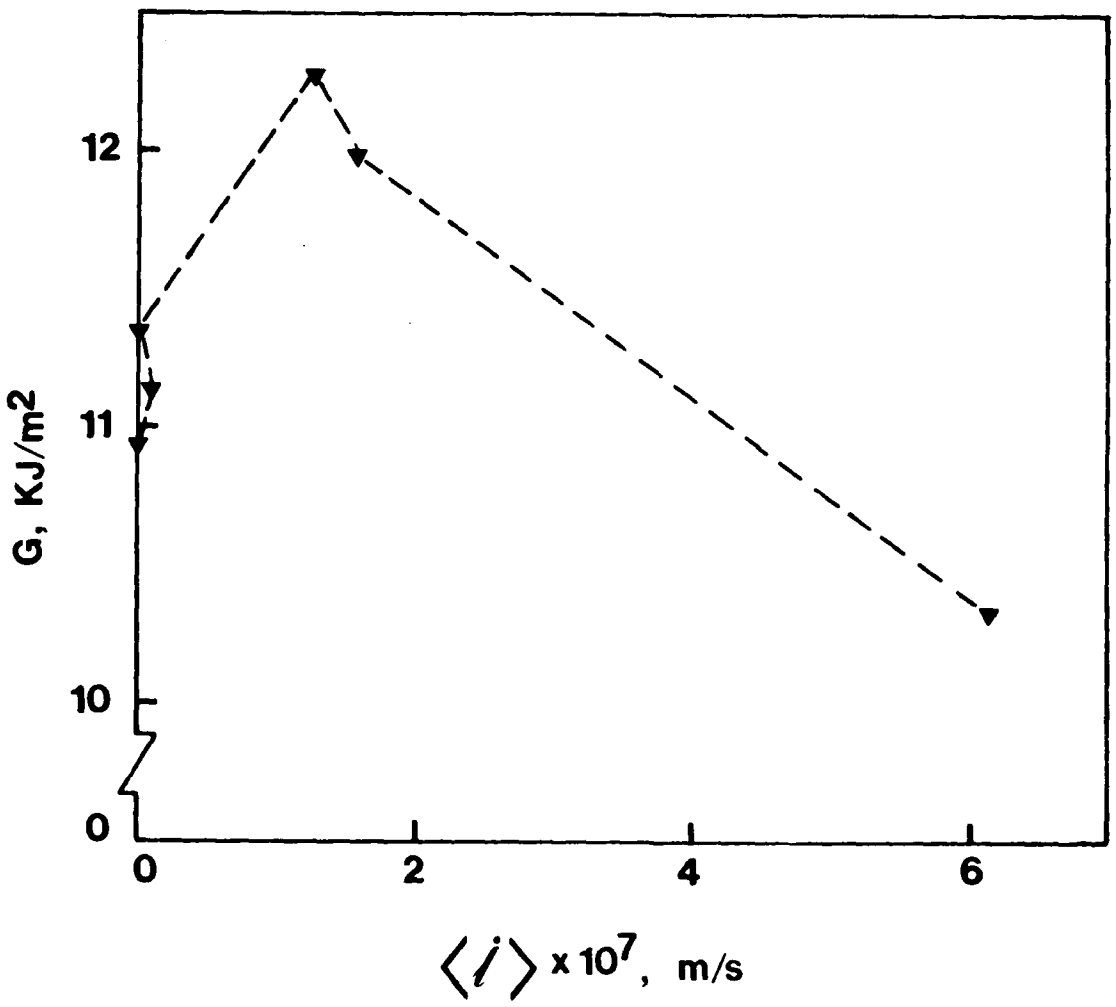
12
11
10
0
G, KJ/m2
0
2
4
6
⟨i⟩ x 10^7, m/s

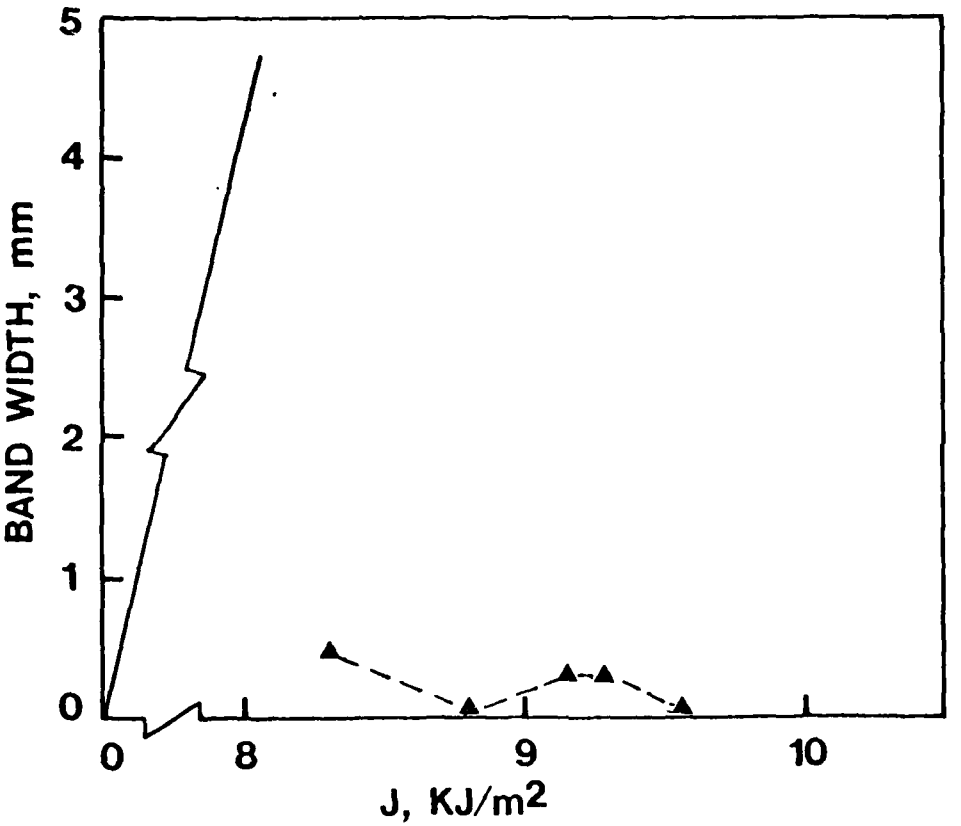
BAND WIDTH, mm
5
4
3
2
1
0
0
8
9
10
J, KJ/m2

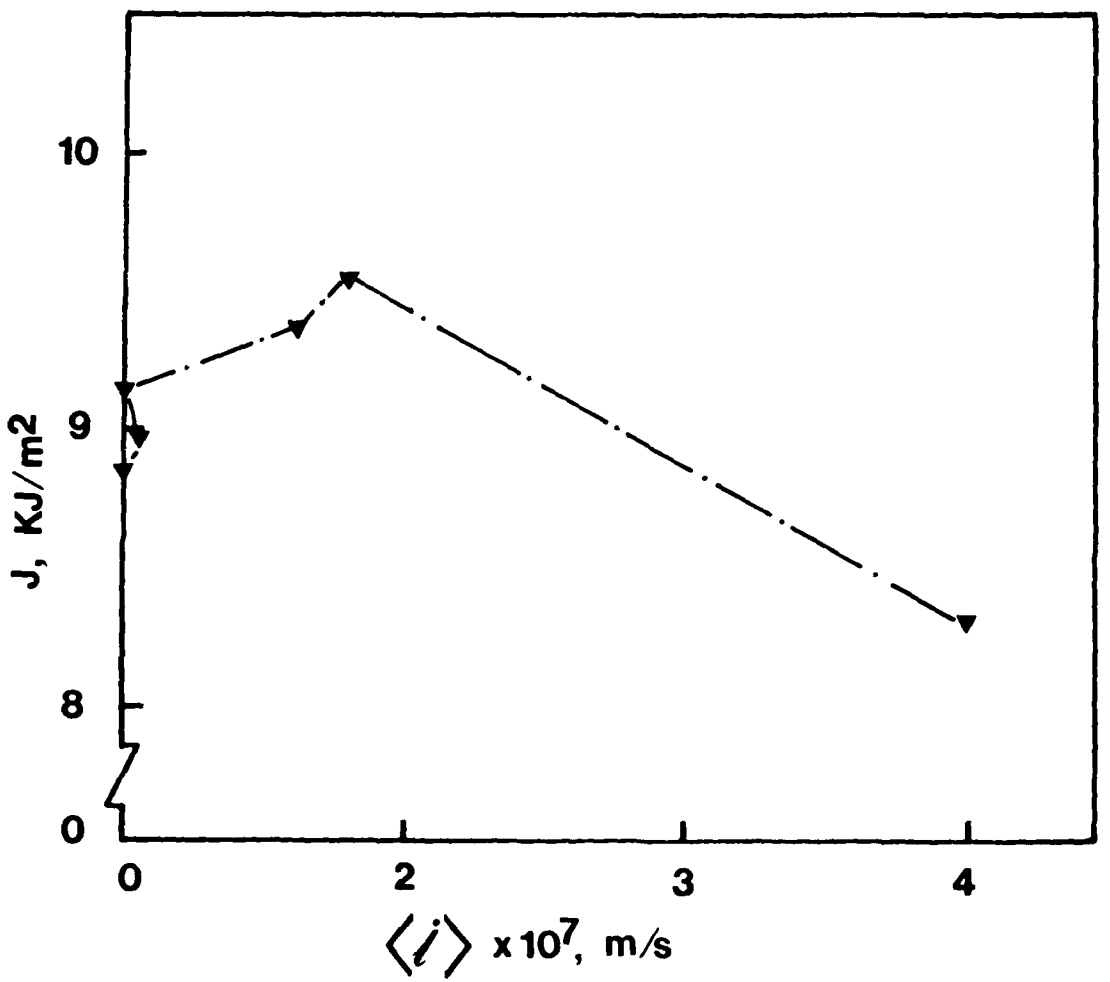
10
9
8
0
J, KJ/m2
0
2
3
4
⟨i⟩ x 10^7, m/s

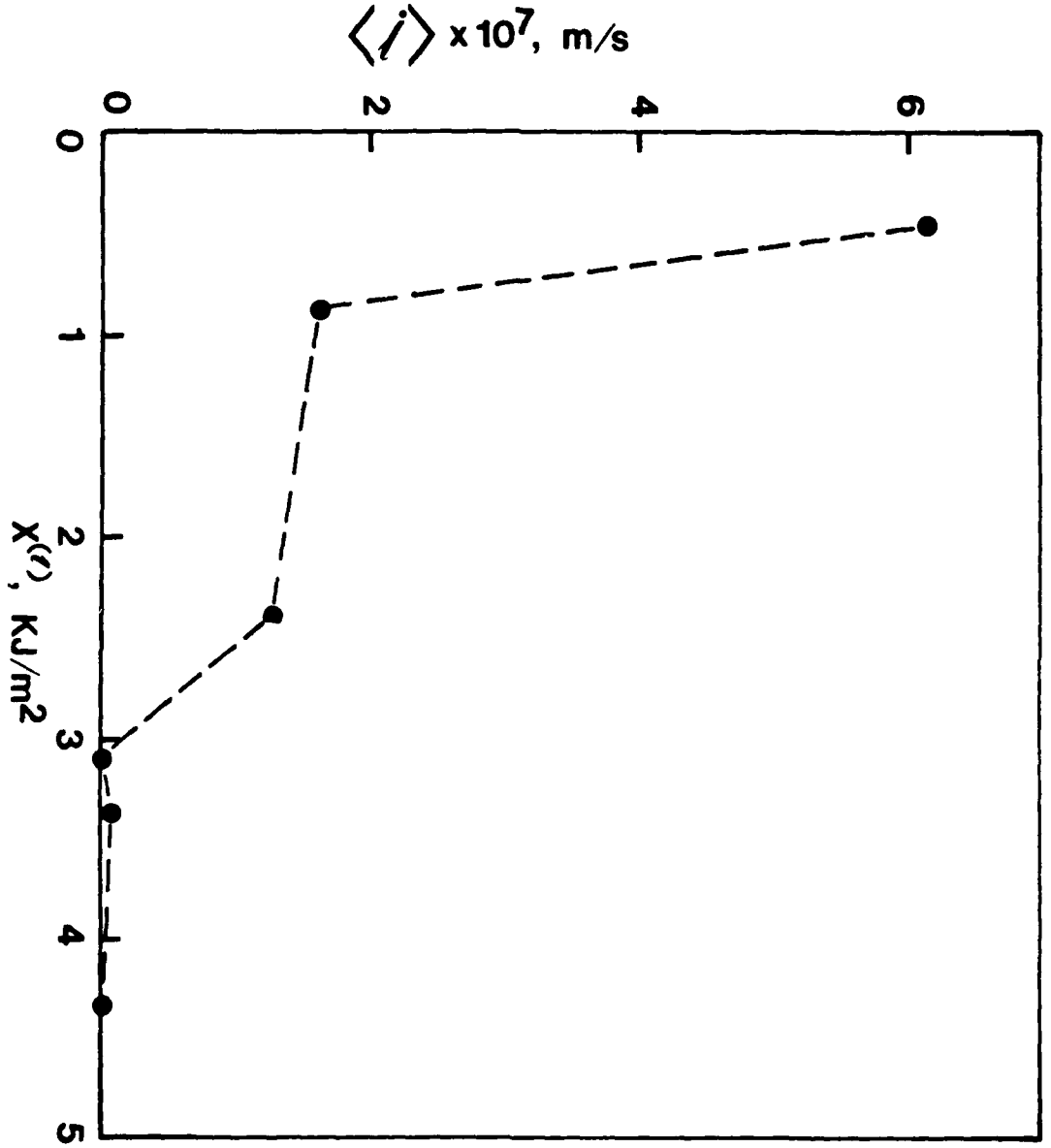
⟨i⟩ x 10^7, m/s
0
2
4
6
0
1
2
3
4
5
X^(r), KJ/m2


NOTCH TIP
2.5 mm


C
NOTCH TIP
2.5 mm
2.5 mm